RSC Advances

PAPER

View Article Online
View Journal | View Issue

Cite this: *RSC Adv.*, 2018, **8**, 19103

Effects of anions on the underpotential deposition behavior of Cu on polycrystalline Pt†

Jiao Liu,[ab] Zhen Xu,[b] Benfeng Zhu,[b] Xiaoqing Du,[b] Yumeng Yang,[b] Chenxi Yi,[b] Zhao Zhang,*[b] Chao Cai[c] and Jianmei Li[c]

Received 30th January 2018
Accepted 7th May 2018

DOI: 10.1039/c8ra00921j

rsc.li/rsc-advances

The process of Cu underpotential deposition (UPD) on polycrystalline Pt (pc Pt) has been investigated by cyclic voltammetry, chronoamperometry and electrochemical impedance spectroscopy techniques using (bi)sulfate and perchlorate (with/without the addition of a small amount of NaCl) as supporting electrolytes, respectively. The results showed that the adsorption capacity of the anions influences both the reversibility and charge transfer resistance (R_{ct}) of Cu UPD reactions on pc Pt. With a negative shift of the applied potential, R_{ct} of the (bi)sulfate system decreases monotonously, whereas R_{ct} of the perchlorate system (with/without Cl^- ions) decreases at first and then increases. Cu UPD on pc Pt follows Langmuir-type adsorption and two-dimensional nucleation/growth mechanisms. The specific adsorption anions ((bi)sulfate and chloride ions) can not only enhance the Cu UPD process by decreasing R_{ct}, but also favor instantaneous 2D nucleation and subsequent grain growth. Finally, the possible deposition mechanisms of the Cu UPD process in the presence of specific adsorption anions were proposed.

1. Introduction

As an opposite concept to overpotential deposition (OPD), underpotential deposition (UPD) has received extensive research interest over many years due to its theoretical and pragmatical significance.[1,2] Generally, the UPD process forms a (sub)monolayer of foreign species on a substrate; therefore, it is especially sensitive to the interfacial state of the electrode/solution and electrolyte composition. Many factors involved in the UPD process (such as the temperature, substrate crystallographic orientation, deposition potential, and the type and concentration of anions or other organic additives) can significantly influence the deposition behavior of UPD species. Among these factors, the effects of anions have attracted great attention and have been extensively studied.

Anions may induce an enhanced Cu UPD process (Cu_{UPD}) or change the electrosorption valency of Cu_{UPD} ad-atoms determined by their adsorption/desorption characteristics;[3] also, the formation of Cu_{UPD}-anion pairs due to anion coadsorption can reduce the coulombic repulsion generated by the partially charged Cu_{UPD} ad-atoms.[3,4] Specific adsorption anions (such as Cl^-, Br^- and SO_4^{2-}) can accelerate the UPD process due to local electrostatic effects,[5,6] the decrease of positive potential in the dense part of the electric double layer (EDL),[7] and possible deformation of the highly stable Cu^{2+} hydration shell caused by the weakly hydrated (bi)sulfate and halide anions (in contrast with perchlorate anions), which can enhance the electron transfer reaction.[5,8] Moreover, the halide adlayer has a significant stabilizing effect on the UPD monolayer.[9] The density and structure of UPD copper on Pt is definitely affected or even dominated by the electrolytic environment; the presence of Cl^- in the electrolyte causes shrinkage of the Cu–Cu distance from 0.285 nm in a pure sulfuric acid environment to 0.259 nm.[10]

To date, considerable studies have concentrated on UPD of Cu on monocrystalline Pt substrates, especially Pt(111)[4,8,11–17] and Pt(110);[5,11] one important aspect of this process is the effects of specific adsorption anions on the structures of the Cu_{UPD} deposits (as well as the anion coadsorption layers) and on the kinetics of the Cu_{UPD} process in acid aqueous solution. In the case of Cu UPD on polycrystalline Pt (pc Pt) substrates, previous studies mainly focused on the effects induced by nonionic additives.[10,18–20] Some nonionic additives (such as acetonitrile and thiourea) influence the Cu UPD processes *via* forming a charged copper-additive complex.[10,18,19] At small concentrations of acetonitrile in a copper sulfate solution ([ACN] $\leq$ 4 mM), adsorbed ACN molecules promote copper underpotential deposition (UPD) on pc Pt.[19] Azo-heterocyclic compounds that bind primarily through a ring nitrogen atom delay UPD processes depending on the bond strength of the adsorbed layer.[20] However, the effect of anions on Cu UPD on pc

[a]*College of Chemistry and Chemical Engineering, Hunan University, Changsha 410082, China*

[b]*Department of Chemistry, Zhejiang University, Hangzhou 310027, China. E-mail: eaglezzy@zju.edu.cn; Tel: +86-13305816563*

[c]*College of Chemistry and Chemical Engineering, Ningxia University, Yinchuan 750021, China*

† Electronic supplementary information (ESI) available. See DOI: 10.1039/c8ra00921j

Pt substrates is also an important aspect for practical applications. Therefore, this paper aims to investigate the effects of anions on Cu_{UPD} behavior on pc Pt using cyclic voltammetry (CV), chronoamperometry (CHR), and electrochemical impedance spectroscopy (EIS) techniques.

2. Experimental

Cu UPD on pc Pt was studied in different aqueous solutions containing (bi)sulfate and perchlorate (with/without the addition of NaCl) ions, respectively. Copper(II) oxide (Alfa Aesar, 99.9995%, metals basis), $CuSO_4$ (Aldrich, ≥99.99%, trace metals basis), H_2SO_4 (Sinopharm, GR), $HClO_4$ (Sinopharm, GR), NaCl (Aladdin, 99.99%, metals basis) and ultrapure water (Millipore Water, resistivity $\rho \geq 18.2$ MΩ cm at 25 °C) were used to prepare the solutions. Unless otherwise stated, all the used ultrapure water was prepared using a Millipore-Q system (Millipore-Q Academic, Millipore, USA) whose source water was doubly distilled in our lab. Immediately before each experiment, all the glassware used was soaked in a chromic mixture overnight and then rinsed with ultrapure water, and all solutions were purged by bubbling with high-purity N_2 for 30 minutes to remove dissolved oxygen.

All experiments were performed in a conventional three-compartment cell at 30 ± 0.1 °C controlled by a thermostatic bath. A pc Pt disk (Pine Research Instrumentation Inc., USA, 99.99%) with a geometric area of 0.1962 cm^2 (the diameter of the circular working area is 5.0 mm) was used as the working electrode, a large platinum foil was used as the counter electrode, and a double liquid junction saturated calomel electrode (SCE) was used as the reference electrode in order to prevent contamination of Cl^- ions. In this paper, all the potentials are referred to SCE. Before each experiment, the pc Pt working electrode was pretreated according to the following procedure: (1) the pc Pt electrode was mechanically polished with 0.5 μm diamond polishing paste to obtain a mirror surface and was then ultrasonically cleaned for 5 min in acetone and ultrapure water, respectively. (2) The pc Pt electrode was transferred into 0.5 M H_2SO_4 to carry out electrochemical polishing (−0.255 V to 1.160 V *vs.* SCE) until the normal CV profile (Fig. 1) appeared. (3) Lastly, the activated pc Pt electrode with a layer of 0.5 M H_2SO_4 solution covering its surface was transferred into the working solution as quickly as possible. After each experiment, the Cu UPD layer was electrochemically stripped; then, the pc Pt electrode was pretreated again according to the above procedure but without mechanical polishing.

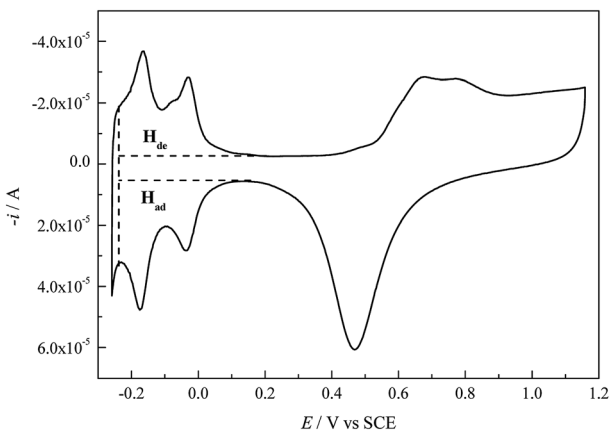

Fig. 1 CV profile obtained for the pc Pt electrode in 0.5 M H_2SO_4 solution at a scan rate (v) of 100 mV s^{-1}.

CV and CHR measurements were carried out using a commercial model electrochemical analyzer/workstation (CHI750D, China). EIS measurements were carried out using an impedance measurement unit (PARSTAT 2273, Advanced Electrochemical System, USA) at different potential biases after the working electrode reached a steady state (~10 minutes). The frequency sweep was always initiated from 100 kHz to 10 MHz with a voltage amplitude of 5.0 mV.

3. Results and discussion

3.1 Cyclic voltammetry

The cleanness of the pc Pt electrode surface was examined by performing CV cycles in 0.5 M H_2SO_4 (Fig. 1). The CV profile is in accordance with that in the literature,[2,21] indicating a clean Pt surface. According to the electric quantity of the H adsorption region (H_{ad}) in Fig. 1 and a theoretical value of 210 μC cm^{-2}, the electrochemical surface area (ECSA) and roughness factor (rf) of the pc Pt electrode were calculated to be 0.3728 cm^{-2} and 1.9 (all the calculations involving the electrode area refer to the apparent area unless otherwise specified), respectively.

Fig. 2 shows the voltammograms for Cu deposition on pc Pt in 1.0 mM Cu^{2+} solutions containing different anions (the CV characteristics of pc Pt in the 5.0 mM Cu^{2+} solutions showed similar behavior to those in the 1.0 mM Cu^{2+} solutions; therefore, they are not shown here). The potential scan always started in the negative direction, and the potential range was between 0.650 V and −0.225 V. In Fig. 2, peak A and B are designated as the bulk deposition and stripping process of Cu deposits, respectively; meanwhile, the enlarged UPD peaks are shown in the insets. The different CV profiles (Fig. 2a–e) reflect significant distinctions of inter-atomic forces between the Cu–Cu and Cu–Pt bondings as well as the distinct energy states of different active sites on the pc Pt surface. From Fig. 2, the potential ranges of the OPD and UPD stripping peaks cover around 100 mV and 500 mV, respectively. Meanwhile, it can also be observed that OPD and its stripping peaks are generally unimodal, whereas UPD and its stripping peaks usually display some humps or broad curves.

Under the conditions of identical Cu^{2+} concentrations, anions exert prominent impacts on both the OPD and UPD processes. With regard to OPD, peaks A and B for the (bi)sulfate supporting electrolyte (Fig. 2a) both appear at more negative potentials than that for the perchlorate supporting electrolyte (Fig. 2b), and the peak current densities of the former are smaller than the latter; this suggests that Cu bulk deposition is more facile in the perchlorate supporting electrolyte. The above phenomena can be attributed to the weaker coordination and adsorption capacity of perchlorate with respect to (bi)sulfate. With increasing Cl^- ions concentration in perchlorate

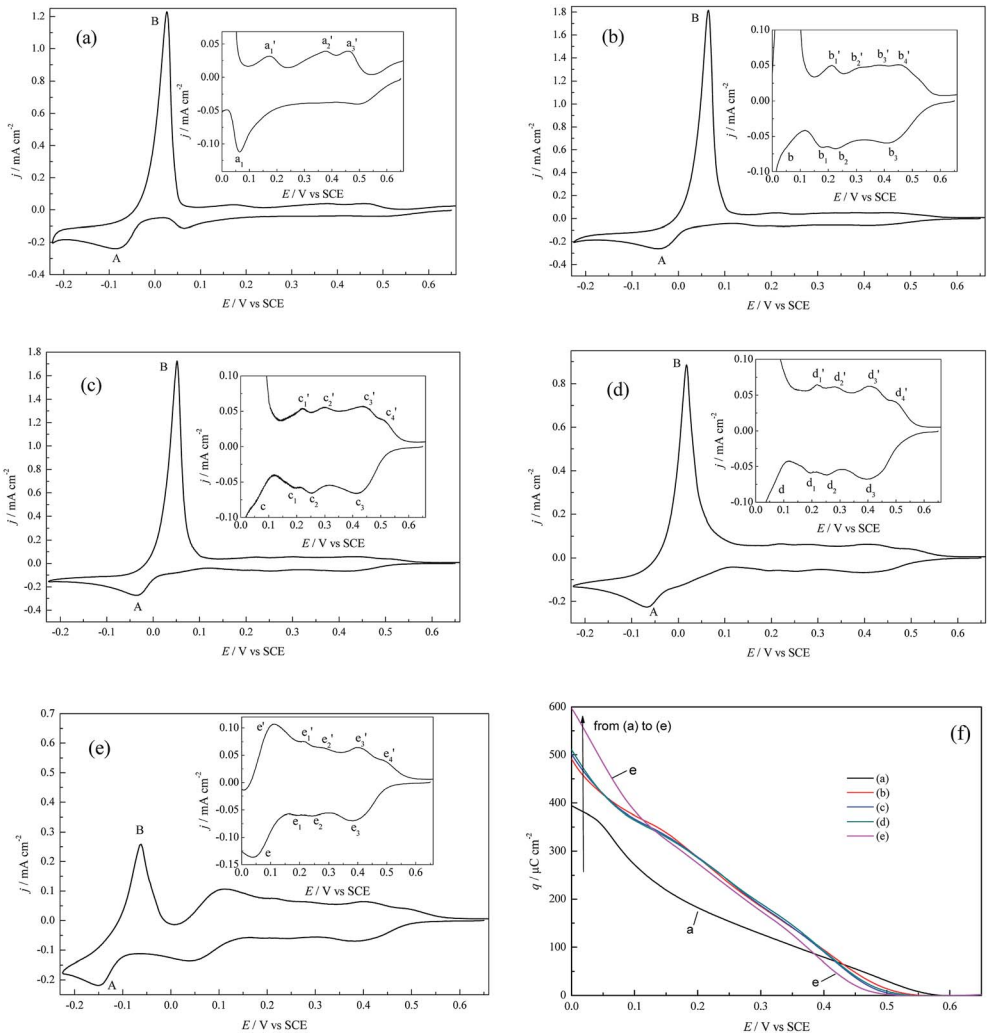

Fig. 2 CV profiles for Cu deposition on pc Pt in (a) 0.5 M H_2SO_4 + 1.0 mM $CuSO_4$, (b) 0.5 M $HClO_4$ + 1.0 mM $Cu(ClO_4)_2$, (c) 0.5 M $HClO_4$ + 1.0 mM $Cu(ClO_4)_2$ + 1.0 mM NaCl, (d) 0.5 M $HClO_4$ + 1.0 mM $Cu(ClO_4)_2$ + 10 mM NaCl, and (e) 0.5 M $HClO_4$ + 1.0 mM $Cu(ClO_4)_2$ + 50 mM NaCl. v = 30 mV s^{-1}. The insets show partial enlarged details of the UPD region. (f) The UPD charge density (q) variation as a function of the applied potentials (E) (the calculations refer to the ECSA), estimated by integrating the voltammograms in Fig. 2a–e.

electrolyte (Fig. 2b–e), the peak potentials of A and B shift negatively and the corresponding peak current densities decrease, whilst the peak shapes experience a gradual change. The above results can be attributed to the strong specific adsorption of Cl^- and the complexation of Cl^- with Cu^{2+} species at higher Cl^- concentrations.[22]

For the UPD process, the CV profiles are much more complicated than for the OPD process; this is attributed to the fact that pc Pt is composed of different crystallographic planes, crystal defects and grain boundaries, and therefore different active sites are in strikingly different energetic states.[23] In (bi) sulfate supporting electrolyte (Fig. 2a), there is only one UPD peak and three stripping peaks, which agrees well with the studies of Alonso *et al.*[24] and also indicates the irreversibility of the Cu UPD process. However, obviously different CV profiles appear in perchlorate supporting electrolyte, and at least three UPD peaks and four stripping humps/peaks appear. For example, in Fig. 2c, in the assignments of UPD and its stripping peaks, peak c_1 should correspond to c_1', peak c_2 to c_2', and peak c_3 to c_3' and c_4'. In the case of the perchlorate supporting electrolyte and Cl^- concentration $c(Cl^-) \leq 10$ mM (Fig. 2b–d), the addition of Cl^- results in more distinct UPD stripping humps and shifts the UPD peak positions towards more positive potentials, suggesting that the Cu_{UPD} process tends to be more facile; however, when $c(Cl^-)$ increases to 50 mM, the boundaries of the UPD humps become inconspicuous and peak e becomes more significant (Fig. 2e).

Fig. 2f shows the variation of the charge density (q) as a function of the applied potential (E). It can be observed that the UPD onset potential is *ca.* 0.56 V for (bi)sulfate electrolyte and *ca.* 0.50 V for perchlorate electrolyte containing 50 mM Cl^-; for q, slight differences can be observed for the perchlorate electrolytes containing lower Cl^- concentrations (0 to 10 mM). In addition, it is interesting to note that the magnitude of q follows the order of q((bi)sulfate) > q(perchlorate) > q(chloride) in the higher potential region (0.43 V to 0.5 V), while the order is

q(chloride) > q(perchlorate) > q((bi)sulfate) in the lower potential region (0.05 V to 0.0 V). Furthermore, almost a full Cu monolayer is completed prior to 0.00 V for perchlorate electrolyte with or without Cl^- according to the q–E relationships (Fig. 2f) (hypothesizing the theoretical charge density needed to form a full Cu monolayer of 420 μC cm^{-2}), which is similar to that of Cu UPD on polycrystalline Au.[25] The differences in q between the (bi)sulfate and perchlorate (with or without Cl^-) systems may synchronously result from the following factors: (1) stronger inductive effects (such as a stronger local electrostatic effect,[5,6] greater potential decrease in the dense part of EDL,[7] possible greater deformation of the hydrated Cu^{2+} hydration shell[5,8]), and more favorable replacement of (bi) sulfate with Cu_{UPD} ad-atoms than perchlorate.[26] (2) Both the different lattice structures in different supporting electrolytes and the different specific adsorption capacities of (bi)sulfate and chloride ions on pc Pt, as well as the complexation of Cu^{2+} species with Cl^- ions, especially at higher Cl^- concentrations. (3) The influence of the electrode potential on the rate and mechanisms of Cu^{2+} charge transfer as well as the desorption rate of the pre-adsorbed anions. For example, in the lower potential region, the perchlorate electrolyte system of 50 mM Cl^- shows the largest q, which may arise from the transition of charge transfer mechanisms due to the complexation of Cl^- ions with Cu^{2+}, such as the transition from single electron transfer ($Cu^{2+} + e \rightarrow Cu^+$, $Cu^+ + e \rightarrow Cu$) to electron transfer coupled with comproportionation ($Cu^+ + Cu^+ \rightarrow Cu + Cu^{2+}$). Shao and his coworkers[22] also reported that the transition between two different mechanisms (direct two-step reduction and the chloride-mediated route) depends on the amount of chloride ions for Cu OPD.

3.2 EIS measurements

With regard to the UPD process, the current density (j_{UPD}) can be expressed as a function of the electrode potential (E), state variables of the electrode surface (X_i), and the surface concentration of UPD species (C_k^s),[27]

$$j_{upd} = f(E, X_i, C_k^s) \quad (1)$$

where the subscripts i and k denote the number of state variables apart from the E and UPD species, respectively. At a small perturbation of the electrode potential, eqn (1) can be expanded using the Taylor series and leaving out the high-order terms,

$$\Delta j_{upd} = \left(\partial j_{upd}/\partial E\right)_{ss}\Delta E + \sum_{i=1}^{x}\left(\partial j_{upd}/\partial X_i\right)_{ss}\Delta X_i + \sum_{k=1}^{y}\left(\partial j_{upd}/\partial C_k^s\right)_{ss}\Delta C_k^s \quad (2)$$

where the subscript "ss" denotes "steady state". Without considering the coadsorption of anions, there should be two state variables, namely the electrode potential (E) and the coverage of UPD species (θ), *i.e.* $i = 1$ and $k = 1$.

$$\Delta j_{upd} = \left(\partial j_{upd}/\partial E\right)\Delta E + \left(\partial j_{upd}/\partial\theta\right)\Delta\theta + \left(\partial j_{upd}\Big/\partial C_{upd}^s\right)\Delta C_{upd}^s \quad (3)$$

Ragoisha's research group[28,29] elaborated several possible equivalent electric circuits (EECs) of EIS when studying the UPD process according to eqn (3). In brief, the right-hand side of eqn (3) indicates the current changes caused by the charge transfer resistance (R_{ct}), adsorption capacitance (C_{UPD}) and mass transfer impedance (Z_T) of the UPD species from left to right, respectively. In view of the reversibility of the UPD process, it can be divided into two different situations. For reversible UPD, the mathematical model of interfacial impedance is expressed as[29–31]

$$Z = R_s + \left\{ Y_0(j\omega)^n + 1\Big/\left[R_{ct} + \left(j\omega C_{upd}\right)^{-1} + Z_T\right]\right\}^{-1} \quad (4)$$

For irreversible UPD, it can be expressed as[29]

$$Z = R_s + \left[Y_0(j\omega)^n + 1/(R_{ct} + Z_T)\right]^{-1} \quad (5)$$

where R_s is the solution resistance. The double layer capacitance is represented by the constant phase-angle element (CPE) because of the general "dispersion effect" for solid electrodes; it is given by $Z_{dl} = Y_0^{-1}(j\omega)^{-n}$, where Y_0 has the dimensions of capacitance related to the EDL and n is a non-dimensional parameter related to the "dispersion effect"; $R_{ct} = -1/(\partial j_{upd}/\partial E)$ is the charge transfer resistance of the UPD process; and the adsorption capacitance C_{UPD} is given by $C_{upd} = -q_{upd}(\partial\theta/\partial E)$, where q_{UPD} and θ denote the charges of the full UPD monolayer and the coverage of the Cu UPD adlayer, respectively. Supposing the coadsorption of specific adsorption anions with different time constants proceeds simultaneously with the Cu UPD process, an additional branch of anion adsorption capacitance (CPE_a) in series with the adsorption resistance (R_a) should be added in parallel with the double layer capacitance.[29,31] Then, for a reversible UPD process,

$$Z = R_s + \left\{ Y_0(j\omega)^n + 1\Big/\left[R_{ct} + \left(j\omega C_{upd}\right)^{-1} + Z_T\right] + 1\Big/\left[R_a + (j\omega C_a)^{-1}\right]\right\}^{-1} \quad (6)$$

For an irreversible UPD process,

$$Z = R_s + \left[Y_0(j\omega)^n + 1/(R_{ct} + Z_T) + 1\Big/\left[R_a + (j\omega C_a)^{-1}\right]\right]^{-1} \quad (7)$$

Potentiodynamic electrochemical impedance spectroscopy (PDEIS) has been applied to study UPD kinetics, of which the ac response must be confined to a limited frequency range while leaving out certain EEC elements, such as mass transfer impedance at low or infralow frequencies.[29] In this study, we adopted the classical EIS technique and decomposed the ac response through the whole EEC in the frequency range between 100 kHz and 10 mHz as much as possible.

3.2.1 Cu UPD in (bi)sulfate electrolyte. Fig. 3a–c show the EIS plots for Cu UPD on pc Pt in 1.0 mM $CuSO_4$ + 0.5 M H_2SO_4 aqueous solution at different applied potentials. The Nyquist diagram (Fig. 3a) is composed of two parts: a high-frequency capacitive arc and a low-frequency oblique line which slightly resembles a large arc. The EIS data shown in Fig. 3a–c were

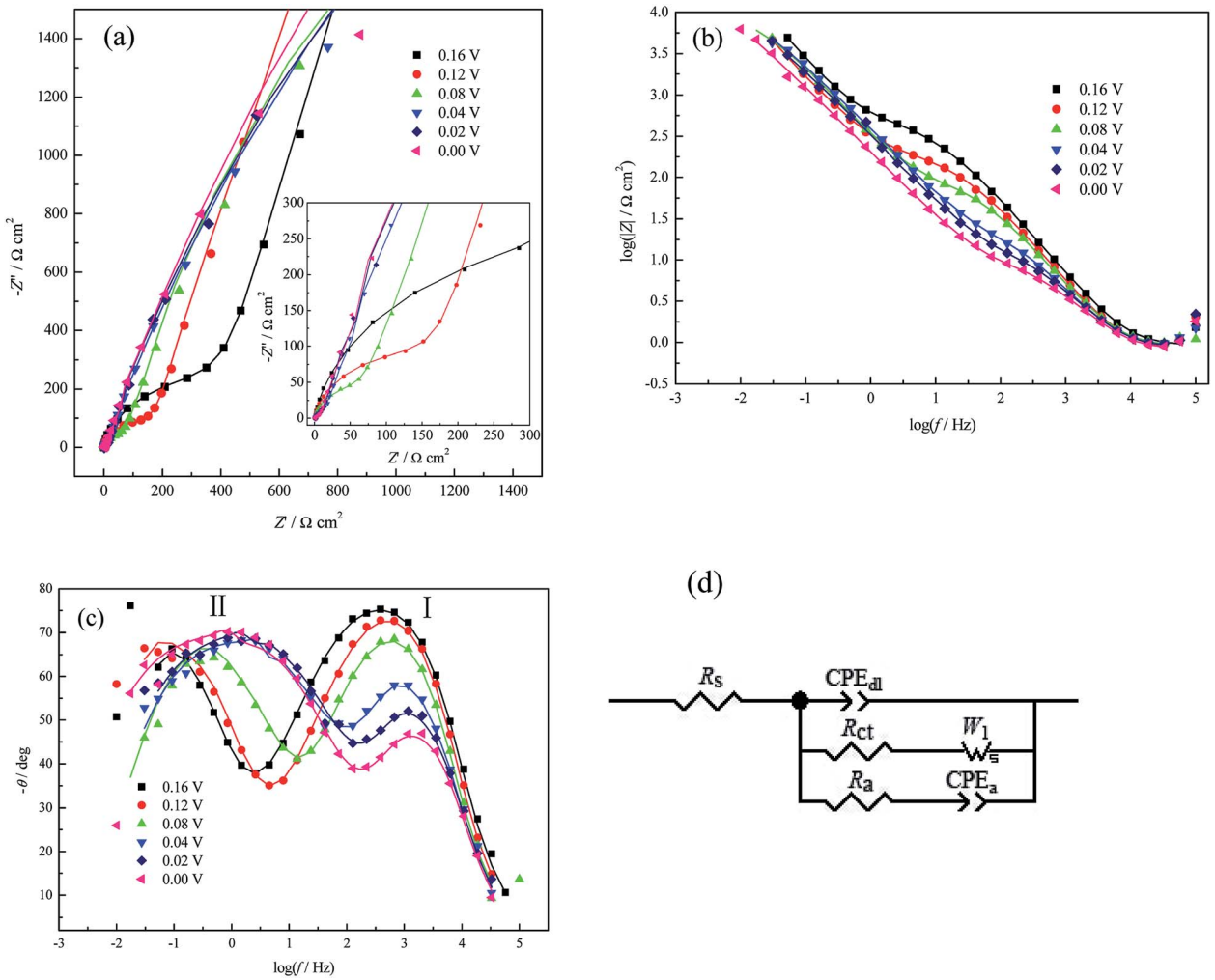

Fig. 3 EIS plots for Cu UPD on pc Pt in 1.0 mM $CuSO_4$ + 0.5 M H_2SO_4 at different potential bias containing both the experimental (symbols) and the fitting results (solid lines). (a) Nyquist plot (inset: enlarged details in the high frequency (HF) range), (b) and (c) Bode plots, and (d) EEC used to fit the impedance data.

fitted with ZView software based on the principle of nonlinear least squares (NLLS fit). The EEC used to fit the impedance data (Fig. 3d) was proposed according to the following considerations: (1) due to the irreversibility of Cu UPD (according to the CV features in Fig. 2a) and the oblique line in the low-frequency region of the Nyquist diagram (Fig. 3a), a branch of charge transfer resistance in series with semi-infinite diffusion impedance was added in parallel with the double layer capacitance. (2) The strong coadsorption of (bi)sulfate in the Cu UPD process is well known. Additionally, the deviation of the inclination angles of the oblique line (Fig. 3a), symbolizing diffusion impedance from $\pi/4$, also demonstrated that the UPD process was affected by other surface state variables (for example, the coverage of the Cu UPD adlayer and (bi)sulfate) in addition to the applied potentials.[27] Thus, an additional branch of adsorption resistance in series with the adsorption capacitance of (bi)sulfate was added in parallel with the double layer capacitance (Fig. 3d). The best fitting parameters are shown in Table 1.

Table 1 EIS fitting results for Cu UPD on pc Pt in 1.0 mM $CuSO_4$ + 0.5 M H_2SO_4 solution

E (V)	R_s (Ω cm^2)	CPE_{dl}-T (μF cm^{-2})	CPE_{dl}-P	R_{ct} (Ω cm^2)	W_1-R (Ω cm^2)	R_a (Ω cm^2)	CPE_a-T (μF cm^{-2})	CPE_a-P
0.16 V	0.921	51.779	0.906	377.881	15 915.744	738.104	337.151	0.912
0.12 V	0.846	58.588	0.916	143.069	15 685.405	265.459	595.158	0.884
0.08 V	0.922	55.708	0.927	23.878	9705.425	95.844	565.240	0.802
0.04 V	0.895	60.112	0.927	13.134	11 956.428	19.973	548.012	0.769
0.02 V	0.890	40.004	0.962	6.530	11 519.294	11.256	673.853	0.778
0.00 V	0.852	42.203	0.967	6.263	17 243.233	7.913	1098.012	0.778

With the negative shift of the applied potentials from 0.16 V to 0.0 V, the diameters of both the high-frequency arc (Fig. 3a) and the impedance module (Fig. 3b) decrease. The frequency of peak I in the Bode plot (Fig. 3c) shifts towards the higher frequency region and the analyzed R_{ct} decreases monotonously (Table 1), which is similar to H UPD in 0.1 M H_2SO_4 solution;[32] this indicates that the UPD process (nucleation/growth) is accelerated and that the formation of Cu_{UPD}-anion pairs due to (bi)sulfate coadsorption decreases the coulombic repulsion caused by the partially charged Cu_{UPD} ad-atoms.[3,4] Meanwhile, two phase angle peaks obviously exist in the Bode plot (Fig. 3c) at all applied potentials, which cannot be observed in PDEIS measurements to a large extent due to its limited sweep frequency range.[28,33–35]

The phase angle value of peak I (Fig. 3c) decreases as the applied potential bias increases (*vs.* open circuit potential (OCP), approximately 0.65 V), which proves that the UPD process becomes more and more nonuniform or inhomogeneous[36] due to the dispersive surface energetic states of pc Pt and the increasing potential bias. The increasing inhomogeneity can also be proved by the decrease of the surface fractal dimensions D_f ($D_f = 3 - n$ or $D_f = 1/n + 1$, where n is the power exponent of the constant phase element, which is CPE_{dl}-P here)[37,38] as the applied potential bias increases. The UPD process caused a slight decrease of the Cu^{2+} concentration (or a slight concentration polarization) based on Faraday's law and the electric quantity consumed by forming a Cu_{UPD} monolayer; meanwhile, the electrode surface should be rationally composed of more Cu_{UPD} and fewer Pt atoms at a higher potential bias (*vs.* OCP) (Fig. 2f). In this case, because both the specific resistance and the area of Pt were smaller than those of the Cu_{UPD} layer, the activity of the residual nude Pt increased gradually with decreasing applied potential; this would certainly accelerate the diffusion process of the UPD species and consequently result in a shift of the low frequency phase angle peak II related to the diffusion process towards the higher frequency region (Fig. 3c). The EIS measurements results at 0.00 V present no sign of inductive components (the shrinkage phenomenon of the real part) in the entire frequency range, which suggests that the H UPD process (or hydrogen evolution

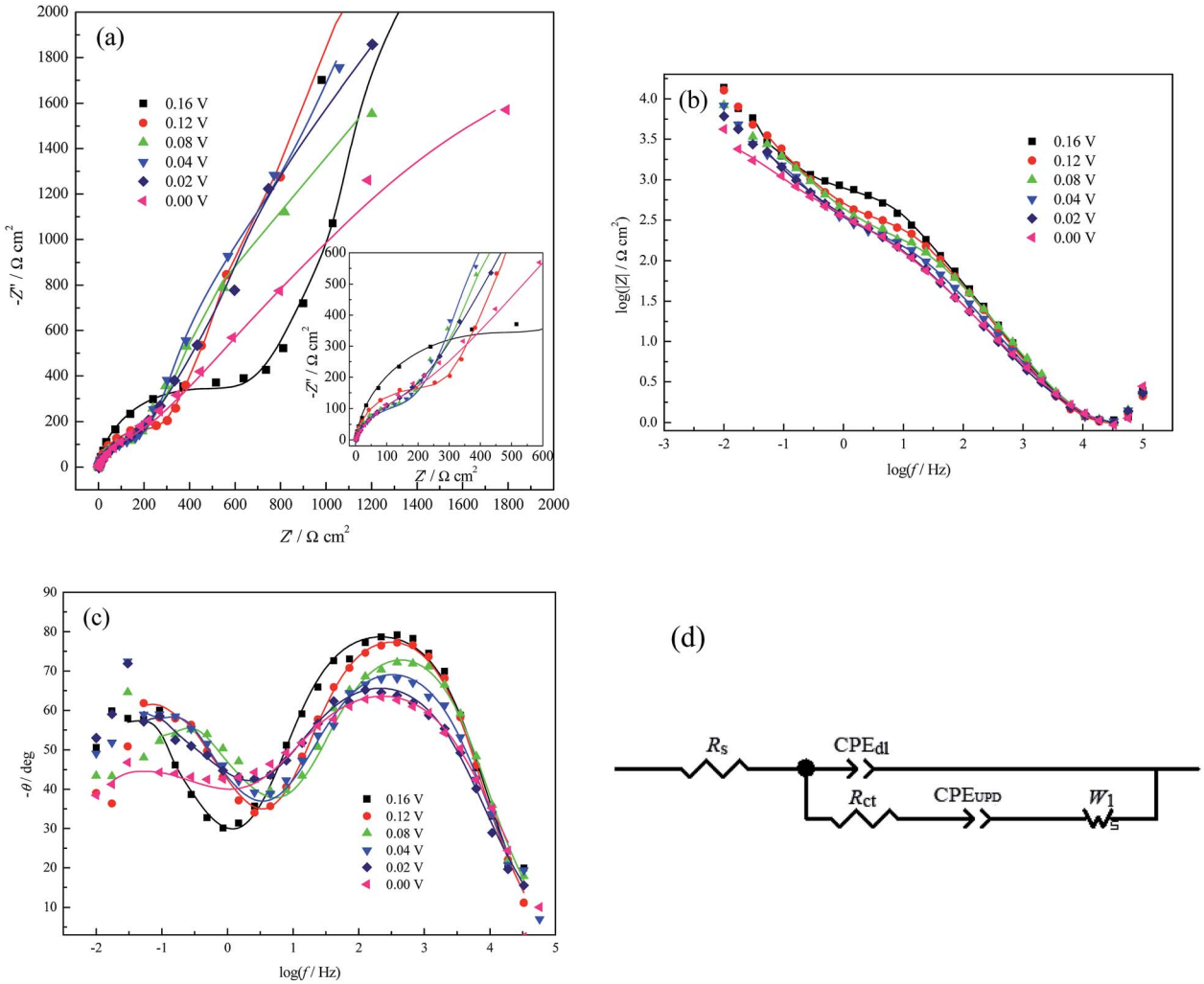

Fig. 4 EIS plots for Cu UPD at pc Pt in 1.0 mM $Cu(ClO_4)_2$ + 0.5 M $HClO_4$ at different potential biases containing both the experimental (symbols) and the fitting results (solid lines). (a) Nyquist plot (inset: enlarged details at HF), (b) and (c) Bode plots, and (d) EEC used to fit the impedance data.

Table 2 EIS fitting results for Cu UPD on pc Pt in 1.0 mM $Cu(ClO_4)_2$ + 0.5 M $HClO_4$ solution

E (V)	R_s (Ω cm^2)	CPE_{dl}-T (μF cm^{-2})	CPE_{dl}-P	R_{ct} (Ω cm^2)	CPE_{UPD}-T (μF cm^{-2})	CPE_{UPD}-P	W_1-R (Ω cm^2)
0.16 V	0.922	49.878	0.921	718.681	843.629	0.746	275.072
0.12 V	0.914	50.177	0.929	322.749	693.323	0.761	755.174
0.08 V	0.900	60.810	0.895	197.573	1045.056	0.774	618.030
0.04 V	0.872	113.216	0.848	206.206	1595.872	0.905	790.294
0.02 V	0.873	203.252	0.797	272.129	1381.244	0.693	1132.663
0.00 V	0.783	242.243	0.769	275.465	1222.477	0.571	2811.546

reaction, HER) is suppressed by Cu UPD. This type of inhibiting phenomenon was also observed for low Cu ad-atoms coverage by Machado and his coworkers.[39]

The fitting results (Table 1) also show that the magnitude of CPE_{dl}-T (*i.e.* Y_0 in eqn (4)) fluctuates within the measurement uncertainties and is much smaller than that of CPE_a-T. This result agrees well with the fact that the former process takes place at the whole electrode/solution interface, while the latter may prefer some active sites for easier adsorption/desorption of (bi)sulfate. Due to the above reasons, it can also be observed that the dispersion index CPE_{dl}-P (*i.e.* n in eqn (4)) is slightly larger than CPE_a-P, and the former is closer to the behavior of pure capacitance. Moreover, the simultaneous increase of CPE_a-T and the applied potential bias (Table 1) further suggests the occurrence of (bi)sulfate adsorption/desorption onto the Cu_{UPD} surface.

3.2.2 Cu UPD in pure perchlorate electrolyte. Fig. 4a–c show the EIS plots for Cu UPD on pc Pt in 1.0 mM $Cu(ClO_4)_2$ + 0.5 M $HClO_4$ aqueous solutions at different potential biases. Similar to the EIS plots of the (bi)sulfate system (Fig. 3), the Nyquist diagram (Fig. 4a) is also composed of a high-frequency capacitive arc and an oblique line (larger arc) appearing in the low or infralow frequency region. Meanwhile, with increasing applied potential bias, both the impedance module (Fig. 4b) and the peak height of the phase angle (Fig. 4c) decrease due to the increasingly inhomogeneous electrode surface.[36] Additionally, the H UPD process (or HER) is also suppressed by the Cu UPD process.

However, for pure the perchlorate electrolyte system, with increasing applied potential bias, the peak frequency of the phase angle (Fig. 4c) initially shows a tendency of a very small shift towards a higher frequency (0.08 V $\leq E \leq$ 0.16 V), then to a lower frequency (0.00 V $\leq E \leq$ 0.08 V); this indicates that the Cu UPD process becomes easier in the range of 0.08 V $\leq E \leq$ 0.16 V and more difficult in the range of 0.00 V $\leq E \leq$ 0.08 V, similar to a recent report.[31] The more difficult UPD process at a larger potential bias may be caused by strong lateral interactions among the partially charged Cu ad-atoms; this can be verified by the q–E dependence (Fig. 2f), where Cu ad-atoms have already reached a relatively large coverage at 0.08 V ($\sim$0.926 monolayer).

The deviation of the inclination angles of the diffusion impedance (Fig. 4a) from $\pi/4$ suggests that the Cu UPD process is affected by other surface state variables in addition to the applied potentials.[27] However, due to the weak adsorption capacity of perchlorate depicted above, the deviation should be mainly attributed to the coverage of the Cu UPD adlayer. Therefore, when simultaneously considering the weak adsorption capacity of perchlorate and the relative reversibility of Cu UPD in the range of 0.00 V $\leq E \leq$ 0.50 V (Fig. 2b, according to the potential difference between the reduction and oxidation peaks[40]), the EEC model (Fig. 4d) proposed by Huang and his coworkers for Cu UPD on polycrystalline Pd[30] was adopted to analyze the EIS data in Fig. 4a–c; the best fitting results are listed in Table 2.

From Table 2, R_{ct} initially decreases and then increases with increasing applied potential bias, which is consistent with the variation of the peak frequency of the phase angle (Fig. 4c). Higher values of R_{ct} are observed in $HClO_4$ solution than in H_2SO_4 solution (Tables 1 and 2), which indicates that the Cu UPD rate in $HClO_4$ solution is slower. This phenomenon is consistent with that observed by Łosiewicz and his coworkers;[32] they also found that H UPD in H_2SO_4 solutions is faster than that in $HClO_4$ solutions. CPE_{dl}-T is much smaller than CPE_{UPD}-T, whilst both CPE_{dl}-T and CPE_{UPD}-T (the fluctuations of their values are within the measurement uncertainties) increase with increasing applied potential bias. The former may be caused by the following synergistic effects: (1) the adsorption capacity of perchlorate is much weaker than that of (bi)sulfate, as proved by the q–E dependence (Fig. 2f), so the Cu UPD process occurs more readily in the perchlorate system with increasing applied potential bias; (2) the strong lateral interactions between the partially charged Cu ad-atoms in the perchlorate system (depicted above) result in a more inhomogeneous (or rougher) electrode surface than the (bi)sulfate system, which can be verified by the decrease of CPE_{dl}-P (Table 2). Meanwhile, CPE_{dl}-T may also be interpreted as the charge–discharge process of the whole electrode/solution interface; however, CPE_{UPD}-T only represents the faradaic pseudo-capacitance occurring at the active sites of the pc Pt surface.

It should be mentioned that the EEC model in Fig. 4d omitting CPE_{UPD} and W_1 was used to fit the PDEIS data[31] when using PDEIS to study Cu UPD on Pt. The obtained R_{ct} values are much larger than those in this paper. The above discrepancies may result from both the dynamic potential scan in the PDEIS measurements and the Cu^{2+} concentration difference.

3.2.3 Cu UPD in perchlorate electrolyte with the addition of Cl^- ions. Fig. 5a–c show the EIS plots for Cu UPD on pc Pt in 1.0 mM $Cu(ClO_4)_2$ + 0.5 M $HClO_4$ + 1.0 mM NaCl aqueous solution at different potential biases; the characteristics (including the evolution features of the EIS plots with the applied potential bias) are very similar to those of the pure

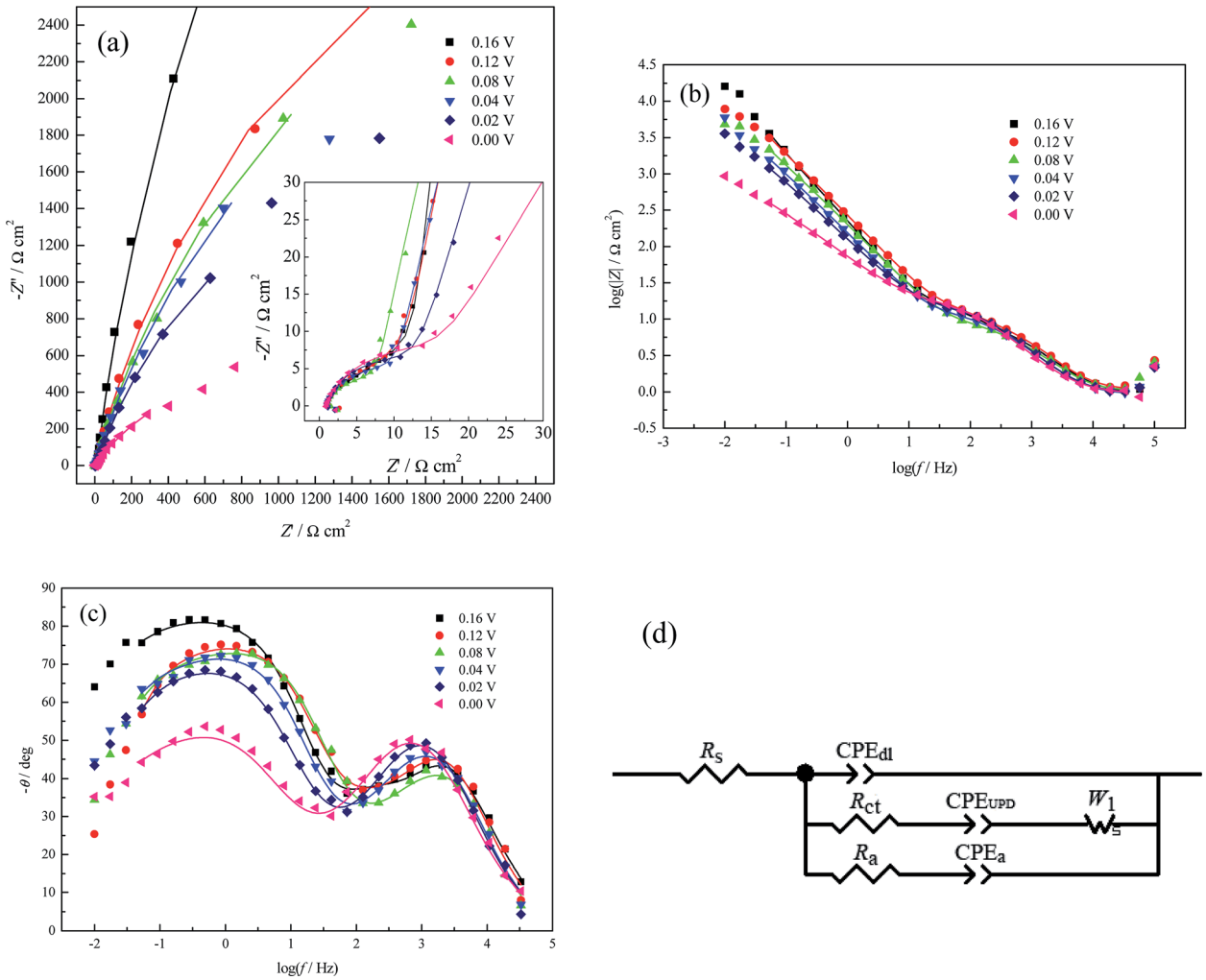

Fig. 5 EIS plots for Cu UPD on pc Pt in 1.0 mM $Cu(ClO_4)_2$ + 0.5 M $HClO_4$ + 1.0 mM NaCl at different potential biases containing both the experimental (symbols) and the fitting results (solid lines). (a) Nyquist plot (inset: enlarged details at HF), (b) and (c) Bode plots, and (d) EEC used to fit the impedance data.

perchlorate system, except that the inclination angles of the diffusion impedance further deviate from $\pi/4$ (insets in Fig. 4a and 5a) due to the comparatively stronger adsorption of Cl^- (than ClO_4^-). Markovic and his coworkers[11] also reported that the specific adsorption capacity of anions at the Pt surface is in the order of chloride > (bi)sulfate > perchlorate, and the bond strength follows the order of Cl^-–Pt > SO_4^{2-}–Pt > ClO_4^-–Pt. When simultaneously considering the reversibility of the Cu UPD process (according to the potential difference between the reduction and oxidation peaks[40] in Fig. 2c) and the strong specific adsorption of Cl^- on pc Pt, the EEC model shown in Fig. 5d was adopted to analyze the EIS data. Table 3 lists the best fitting results.

From Table 3, R_{ct} initially decreases and then increases with increasing applied potential bias. This variation trend of R_{ct} is very similar to that in a pure perchlorate electrolyte bath (Table

Table 3 EIS fitting results for Cu UPD on pc Pt in 1.0 mM $Cu(ClO_4)_2$ + 0.5 M $HClO_4$ + 1.0 mM NaCl solution

E (V)	R_s (Ω cm^2)	CPE_{dl}-T (μF cm^{-2})	CPE_{dl}-P	R_{ct} (Ω cm^2)	CPE_{UPD}-T (μF cm^{-2})	CPE_{UPD}-P	W_1-R (Ω cm^2)	R_a (Ω cm^2)	CPE_a-T (μF cm^{-2})	CPE_a-P
0.16	0.926	119.893	0.850	13.065	82.768	0.906	63 060.642	17.162	590.826	0.950
0.12	1.052	80.459	0.887	11.674	349.725	0.720	6876.810	20.424	359.516	0.938
0.08	1.055	28.836	0.997	3.588	538.481	0.666	2505.866	10.614	558.716	0.922
0.04	0.925	75.474	0.918	4.573	624.720	0.601	1235.079	13.987	811.009	0.914
0.02	0.950	142.961	0.864	14.697	605.861	0.526	1988.487	17.020	1202.548	0.866
0.00	0.929	280.133	0.810	26.153	1980.581	0.784	1146.200	36.297	2482.875	0.463

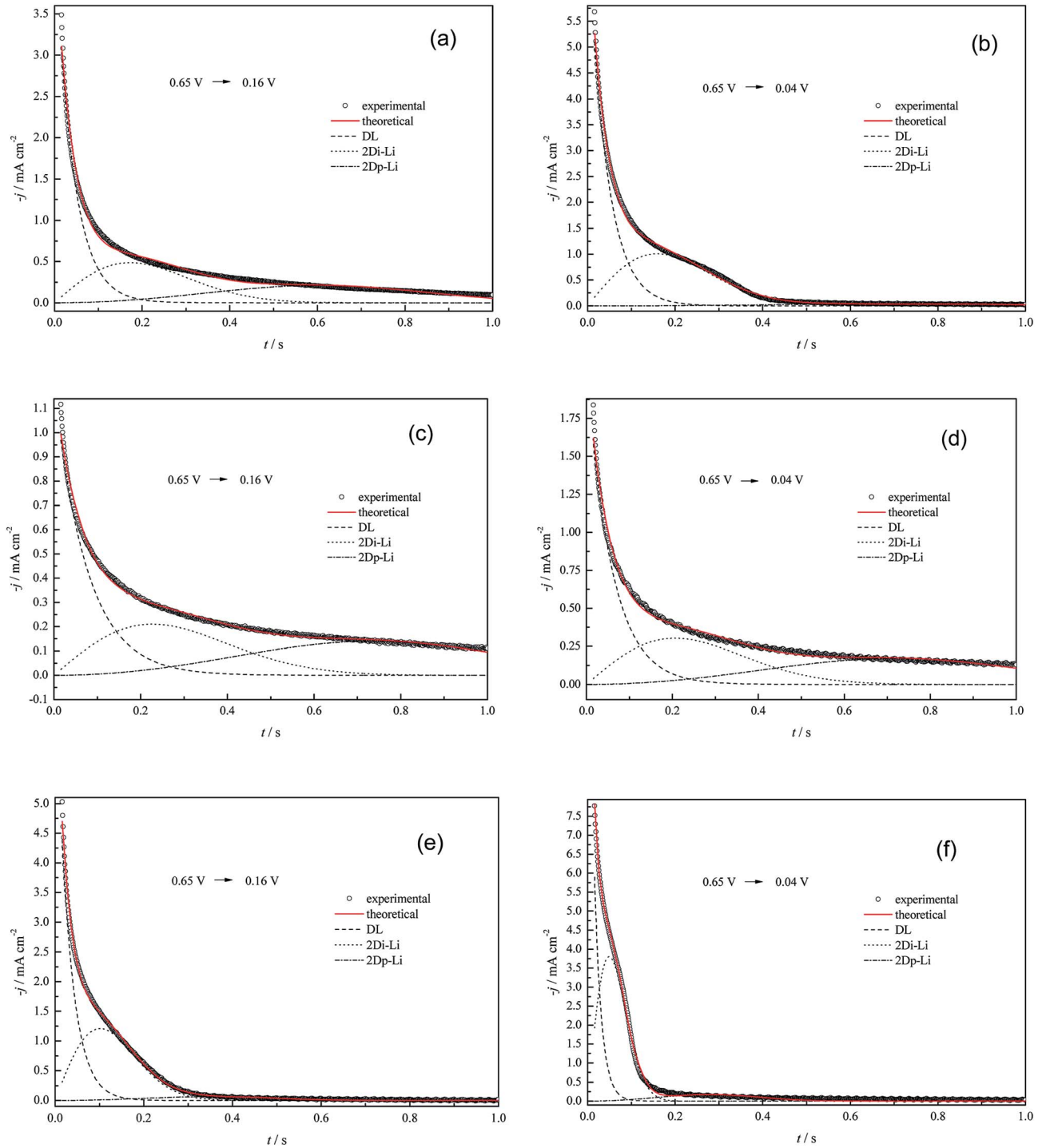

Fig. 6 Experimental current density transients recorded for Cu UPD at pc Pt in (a) and (b) 5.0 mM $CuSO_4$ + 0.5 M H_2SO_4, (c) and (d) 5.0 mM $Cu(ClO_4)_2$ + 0.5 M $HClO_4$, (e) and (f) 5.0 mM $Cu(ClO_4)_2$ + 0.5 M $HClO_4$ + 1.0 mM NaCl, and theoretical non-linear fitting with eqn (15) at some selected potentials. Other current density transients with non-linear fitting results shown in the ESI (Fig. S1–S3†).

2); the reason for this has been elucidated in Section 3.2.2. However, this variation trend of R_{ct} is very different from that in (bi)sulfate electrolyte (Table 1), which can be attributed to the different effects of perchlorate and (bi)sulfate ions on the Cu UPD process. Table 3 also clearly shows that R_{ct} is slightly smaller than R_a, indicating more facile adsorption of Cu_{UPD} adatoms than Cl^- ions. From Table 3, CPE_{dl}-T is much smaller than both CPE_{UPD}-T and CPE_a-T; this is because CPE_{dl}-T, CPE_{UPD}-T and CPE_a-T originate from the whole electrode/solution interface, the fast charge transfer reaction (*i.e.* pseudo-capacitance) and the strong adsorption/desorption of Cl^- ions at the active sites, respectively.

3.3 Potentiostatic current transient measurements

The aim of this section is to investigate the effects of anions (SO_4^{2-}, ClO_4^- and Cl^-) on the nucleation and growth features of the Cu UPD process, and solutions containing 5.0 mM Cu^{2+} with specific anions were chosen to perform chronoamperometric (CHR) experiments (Fig. 6). Additionally, in order to avoid the pre-adsorption of dissolved oxygen species and Cu UPD adatoms, the potential for the remaining CHR tests was selected as 0.65 V. Potentiostatic current density transients were obtained by voltage stepping from the rest potential to the UPD potentials.

There are two typical differences between the "*j*–*t*" curves of different electrolyte systems (Fig. 6). One is that an obvious shoulder peak always exists for all the "*j*–*t*" curves obtained in the perchlorate electrolyte system containing 1.0 mM Cl^- ions, whereas this peak does not appear in the pure perchlorate electrolyte system or only exists at higher potential biases for the (bi)sulfate electrolyte system. The other difference is that the current density (after the initial marked drop, which is simultaneously related to charging of the adsorption pseudocapacitance, *i.e.* the discharging of copper ions in the copper electrodeposition process,[41,42] or the shoulder peak) is much larger than zero for the pure perchlorate electrolyte system, whereas it always levels off to zero for the perchlorate electrolyte system containing 1.0 mM Cl^- ions or for the (bi)sulfate electrolyte system at higher potential biases (the critical potential is *ca.* 0.04 V).

Currently, it is widely accepted that the UPD process generally follows the two-dimensional (2D) nucleation/growth mechanism.[43,44] According to the j_p–$v^{1/2}$ relationship in Fig. 7, linear fitting results reveal that the rate-controlling step of Cu UPD with diffusion control was converted to non-diffusion control as a result of the increase of the Cu^{2+} concentration from 1.0 mM to 5.0 mM. On the other hand, based on the fact that the formation of even an integrated Cu_{UPD} monolayer only consumes 8.11×10^{-7} mM Cu^{2+} in our experimental conditions (hypothesizing a two-electron transfer mechanism), the Cu UPD process should be mostly controlled by charge transfer. Therefore, the theoretical models proposed by Bewick–Fleischmann–Thirsk (BFT) were adopted to analyze the current density transients shown in Fig. 6. In the BFT model, the overlapping effects between crystal nuclei are taken into consideration, and the growth of the 2D circular island nuclei proceeds with lattice incorporation of adatoms into the periphery of the growing nuclei as the rate-controlling step.[45,46] According to the BFT model, the nucleation/growth current densities of 2D instantaneous nucleation (2Di-Li) and 2D progressive nucleation (2Dp-Li) are given by the following equations, respectively.[25,45,46]

$$j_{2Di\text{-}Li}(t) = k_1 t \exp(-k_2 t^2) \quad (8)$$

$$j_{2Dp\text{-}Li}(t) = k_3 t^2 \exp(-k_4 t^3) \quad (9)$$

where $k_1 = 2\pi zFMhN_0{k_g}^2/\rho$, $k_2 = \pi N_0 M^2 {k_g}^2/\rho^2$, $k_3 = \pi zFMhAN_0{k_g}^2/\rho$, and $k_4 = \pi A N_0 M^2 {k_g}^2/(3\rho^2)$; zF denotes the molar charge transferred during the deposition process (C mol^{-1}); M is the atomic weight (g mol^{-1}); h is the layer height (cm); N_0 is the number density of active sites (cm^{-2}); k_g is the lateral growth rate constant (mol cm^{-2} s^{-1}); t is the deposition time (s); ρ is the density of the deposit (g cm^{-3}); and A is the nucleation rate constant (s^{-1}).

The deposition process should accompany the deposition/dissolution of metal ions/metal adatoms, namely, the copper ion discharge process. Milchev *et al.*[41,42] have shown that discharge of the copper ions takes place in two steps:

$$Cu^{2+} + e \rightarrow Cu^+ \quad (10)$$

$$Cu^+ + e \rightarrow Cu \quad (11)$$

Meanwhile, assuming that the deposition/dissolution of a (sub)monolayer at defect sites mostly resembles a Langmuir-type adsorption/desorption process, the current density can be expressed as:[41–43,45,47]

$$j_{ad}(t) = k_5 \exp(-k_6 t) \quad (12)$$

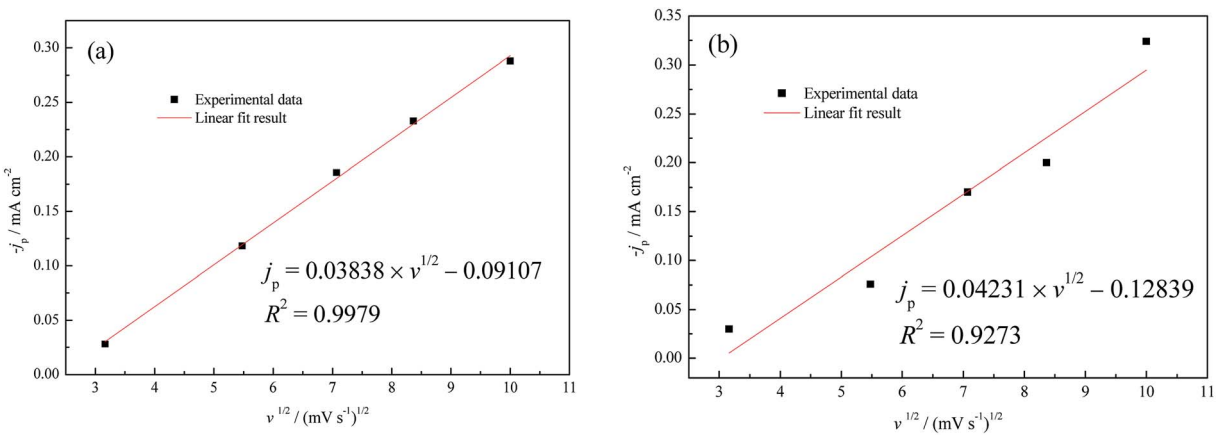

Fig. 7 UPD peak maxima j_p of CV in (a) 0.5 M H_2SO_4 + 1.0 mM $CuSO_4$, (b) 0.5 M H_2SO_4 + 5.0 mM $CuSO_4$ as a function of the square root of the scan rate (v).

For the deposition of metal ions associated with a charge transfer,[43]

$$k_6 = k_a^0 \exp[-(1-\beta)nFE/RT] \quad (13)$$

For the dissolution of metal adatoms,[43]

$$k_6 = k_d^0 \exp(\beta nFE/RT) \quad (14)$$

where k_6 is assumed to follow the Butler–Volmer relation, β is the transfer coefficient, and k_a^0 and k_d^0 denote the standard rate constants of the deposition and dissolution processes, respectively. Thus, in consideration of the Langmuir-type adsorption/desorption process proceeding in parallel with the nucleation and growth process of Cu UPD on pc Pt, the total current density transient should be theoretically decomposed into three parts: double layer charging accompanied by faradaic pseudo-capacitance, two-dimensional instantaneous nucleation (2Di-Li) and two-dimensional progressive nucleation (2Dp-Li):

$$j_{total}(t) = j_{ad}(t) + j_{2Di\text{-}Li}(t) + j_{2Dp\text{-}Li}(t) \quad (15)$$

The experimental current density transients were deconvolved by non-linear fitting with eqn (15), and the fitted lines are also shown in Fig. 6. Based on the best fitting parameters k_1 to k_6 (shown in the ESI of this paper, Tables S1–S3†), the electric quantities of the different contributions (Q_{ad}, $Q_{2Di\text{-}Li}$ and $Q_{2Dp\text{-}Li}$) were calculated according to expressions (16)–(18)[25] and are listed in Tables 4–6

$$k_5 = Q_{ad}k_6 \quad (16)$$

$$k_1 = 2Q_{2Di\text{-}Li}k_2 \quad (17)$$

$$k_3 = 3Q_{2Dp\text{-}Li}k_4 \quad (18)$$

In eqn (16)–(18) and Tables 4–6, Q_{ad}, $Q_{2Di\text{-}Li}$ and $Q_{2Dp\text{-}Li}$ are the charge densities of adsorption, 2D instantaneous nucleation/growth and progress nucleation/growth, respectively; $Q_{nucl} = Q_{2Di\text{-}Li} + Q_{2Dp\text{-}Li}$, $Q_{total} = Q_{ad} + Q_{nucl}$; q_{ad} and q_{nucl} are the contributions of adsorption and nucleation to the total charge density, respectively.

For Cu UPD in the above three systems, Q_{total} always increases with increasing applied potential bias (Tables 4–6). However, comparing the values of Q_{total}, Q_{ad} and q_{ad} of different systems, it is interesting to observe that all of them are directly related to the anionic specific adsorption capacity. Briefly, the stronger the adsorption capacity of the anions in the supporting

Table 4 Charge density and proportion of different contributions to Cu UPD on pc Pt in 5.0 mM $CuSO_4$ + 0.5 M H_2SO_4 in terms of eqn (16)–(18)

E (V)	Q_{ad} (μC cm^{-2})	$Q_{2Di\text{-}Li}$ (μC cm^{-2})	$Q_{2Dp\text{-}Li}$ (μC cm^{-2})	Q_{nucl} (μC cm^{-2})	Q_{total} (μC cm^{-2})	q_{ad} (%)	q_{nucl} (%)
0.16	186.110	138.844	123.901	262.745	448.855	41.463	58.537
0.12	210.807	173.477	138.821	312.298	523.105	40.299	59.701
0.08	218.230	187.258	163.011	350.269	568.499	38.387	61.613
0.04	315.751	263.973	26.615	290.588	606.339	52.075	47.925
0.02	247.359	170.395	211.423	381.818	629.177	39.315	60.685
0.00	307.161	300.887	33.151	334.038	641.199	47.904	52.096

Table 5 Charge density and proportion of different contributions to Cu UPD on pc Pt in 5.0 mM $Cu(ClO_4)_2$ + 0.5 M $HClO_4$ in terms of eqn (16)–(18)

E (V)	Q_{ad} (μC cm^{-2})	$Q_{2Di\text{-}Li}$ (μC cm^{-2})	$Q_{2Dp\text{-}Li}$ (μC cm^{-2})	Q_{nucl} (μC cm^{-2})	Q_{total} (μC cm^{-2})	q_{ad} (%)	q_{nucl} (%)
0.16	91.034	78.841	100.757	179.598	270.632	33.637	66.363
0.12	78.721	69.486	82.852	152.338	231.059	34.070	65.930
0.08	111.169	95.960	114.182	210.141	321.310	34.599	65.401
0.04	122.454	103.243	119.615	222.858	345.312	35.462	64.538
0.02	133.165	108.358	117.791	226.149	359.314	37.061	62.939
0.00	179.900	147.879	152.242	300.122	480.022	37.478	62.522

Table 6 Charge density and proportion of different contributions for Cu UPD at pc Pt in 5.0 mM $Cu(ClO_4)_2$ + 0.5 M $HClO_4$ + 1.0 mM NaCl in terms of eqn (16)–(18)

E (V)	Q_{ad} (μC cm^{-2})	$Q_{2Di\text{-}Li}$ (μC cm^{-2})	$Q_{2Dp\text{-}Li}$ (μC cm^{-2})	Q_{nucl} (μC cm^{-2})	Q_{total} (μC cm^{-2})	q_{ad} (%)	q_{nucl} (%)
0.16	225.323	202.359	22.257	224.616	449.939	50.079	49.921
0.12	237.648	240.819	16.953	257.772	495.420	47.969	52.031
0.08	245.331	286.739	24.954	311.692	557.024	44.043	55.957
0.04	256.258	309.797	47.260	357.057	613.315	41.782	58.218
0.02	276.591	305.269	64.873	370.142	646.734	42.767	57.233
0.00	586.859	47.097	95.063	142.160	729.019	80.500	19.500

electrolyte, the larger the parameters (Q_{total}, Q_{ad} and q_{ad}). For the systems containing SO_4^{2-} (Table 4) and Cl^- (Table 6) ions with stronger adsorption capacity, $Q_{2Di\text{-}Li}$ is generally larger than $Q_{2Dp\text{-}Li}$ (except at the potentials adjacent to the Nernst potential; the reason for this is under further investigation), and the differential of $Q_{2Di\text{-}Li}$ and $Q_{2Dp\text{-}Li}$ increases with increasing anionic specific adsorption capacity. Meanwhile, for the pure perchlorate supporting electrolyte system (Table 5), $Q_{2Di\text{-}Li}$ is always slightly smaller than $Q_{2Dp\text{-}Li}$, and the differential of q_{nucl} and q_{ad} is significantly larger than that obtained in the systems containing SO_4^{2-} or Cl^- ions. The above results undoubtedly indicate that the process of Cu UPD on pc Pt is always coupled with adsorption and replacement of the used anions, and the anions with stronger adsorption capacity facilitate the process of instantaneous nucleation and subsequent growth. When simultaneously taking into account the results shown in Fig. 2, it is rational to consider that co-adsorbed Cu_{UPD}^{n+} – anions (n = 0 to 2) of some specific structures should exist on the pc Pt surface and influence the deposition rate to some extent.

The UPD process is highly complicated, and the deposition mechanisms should be mainly related to both the spatial structures of the adsorbed anions and the electrostatic interactions of the anions with the substrate and UPD species. Based on the above results and the previous reports of Cu UPD on single crystal Pt concurrent with coadsorption of specific adsorption anions,[5,8,12,13,48] it is rational to deduce that Cu UPD on a pc Pt surface in the presence of specific adsorption anions may proceed *via* the following mechanisms. Firstly, before the onset potential of Cu UPD, the specific adsorption anions adsorb onto the Pt substrate and gradually translate into specific adlayers of certain lattice structures (the structures may transform along with the negative potential scan), which will also deform the hydration shell of the pre-adsorbed Cu^{2+} (some specific adsorption anions can even insert into the Cu^{2+} hydration shells) and cause a decrease of the positive potential in the dense part of the EDL region.[7] Meanwhile, the electrostatic interaction of the specific adsorption anions with Cu^{2+} ions causes the latter to gather in the dense part of the EDL. Secondly, when the UPD potential is suddenly applied, Cu UPD proceeds with simultaneous replacement of the adsorbed anions at certain active sites,[26] and some uniform structures of co-adsorbed Cu_{UPD}^{n+} – anion (n = 0 to 2) may form at some critical potentials. Here, it should be mentioned that in the presence of halide ions, Pb UPD on pc Au may proceed *via* the reduction of Pb^{2+} adsorbed on the pre-adsorbed halide ions.[49] Finally, as the potential becomes more negative, the UPD process continues until the integrated Cu UPD monolayer is formed; this process is always coupled with the adsorption of specific adsorption anions onto the Cu UPD monolayer (a sandwiched structure), which may inhibit the continuous deposition of Cu^{2+} on the Cu_{UPD} layer, thereby stabilizing the UPD film.[10,13]

4. Conclusions

The CV plot of pc Pt in a (bi)sulfate system shows only one significant UPD peak and three corresponding stripping peaks; this differs from the plots of perchlorate systems, which contain at least three UPD peaks and four stripping peaks. In contrast to the irreversibility of the Cu UPD process in the (bi)sulfate system, better reversibility was observed in the perchlorate system, and the reversibility was further improved by the addition of a small amount of Cl^- ions.

Anions with stronger adsorption capacity facilitate the process of 2D instantaneous nucleation and subsequent grain growth, and specific adsorption anions ((bi)sulfate and chloride) can enhance the Cu UPD process by decreasing the charge transfer resistance (R_{ct}). With decreasing applied potential, R_{ct} of the (bi)sulfate system decreases monotonously, whereas R_{ct} shows a trend of initial decrease and subsequent increase for perchlorate systems with or without Cl^- ions. Finally, the possible mechanisms of Cu UPD on pc Pt in the presence of specific adsorption anions were proposed; these reveal the intrinsic relationships between specific adsorption anions and the Cu UPD process.

Conflicts of interest

There are no conflicts to declare.

Acknowledgements

This work was financially supported by the National Natural Science Foundation of China (Project 21273199, 51771173, 51741107).

References

1 Z. Xu, Y. Chen, Z. Zhang and J. Zhang, *Acta Phys.-Chim. Sin.*, 2015, **31**, 1219–1230.
2 Z. Xu, D. M.Qi, L. Jiang, Y. Chen, Z.Zhang and J. Zhang, *Acta Phys.-Chim. Sin.*, 2015, **31**, 1231–1250.
3 C. Wang, C. S. Chung and S. C. Chang, *J. Electroanal. Chem.*, 1995, **395**, 317–321.
4 H. S. Yee and H. D. Abruna, *Langmuir*, 1993, **9**, 2460–2469.
5 B. Grgur, C. Lucas and P. Ross, *Electrochim. Acta*, 1998, **44**, 1009–1017.
6 A. I. Danilov, E. B. Molodkina, Y. M. Polukarov, V. Climent and J. M. Feliu, *Electrochim. Acta*, 2001, **46**, 3137–3145.
7 A. Danilov, E. Molodkina and Y. M. Polukarov, *Russ. J. Electrochem.*, 2000, **36**, 976–986.
8 N. M. Markovic, H. A. Gasteiger and P. N. J. Ross, *Langmuir*, 1995, **11**, 4098–4108.
9 Y. Gründer, P. Thompson, A. Brownrigg, M. Darlington and C. A. Lucas, *J. Phys. Chem. C*, 2012, **116**, 6283–6288.
10 M. Wünsche, H. Meyer and R. Schumacher, *Electrochim. Acta*, 1995, **40**, 629–635.
11 N. Markovic and P. Ross, *Langmuir*, 1993, **9**, 580–590.
12 N. M. Markovic, C. Lucas, H. A. Gasteiger and P. Ross, *Solid-Liquid Electrochemical Interfaces*, 1997, vol. 656, pp. 87–105.
13 H. Ogasawara, J. Inukai and M. Ito, *Surf. Sci.*, 1994, **311**, L665–L670.

14 Y. Soldo, E. Sibert, G. Tourillon, J. L. Hazemann, J. Lévy, D. Aberdam, R. Faure and R. Durand, *Electrochim. Acta*, 2002, **47**, 3081–3091.
15 C. Lucas, N. Marković, I. Tidswell and P. Ross, *Phys. Rev. B: Condens. Matter Mater. Phys.*, 1996, **221**, 245–250.
16 N. M. Marković, H. A. Gasteiger, C. A. Lucas, I. M. Tidswell and P. N. Ross Jr, *Surf. Sci.*, 1995, **335**, 91–100.
17 I. Tidswell, C. Lucas, N. Marković and P. Ross, *Phys. Rev. B*, 1995, **51**, 10205.
18 A. V. Rudnev, T. Zapryanova, E. B. Molodkina, A. I. Danilov and Y. M. Polukarov, *Russ. J. Electrochem.*, 2008, **44**, 840–846.
19 A. V. Rudnev, E. B. Molodkina, A. I. Danilov and Y. M. Polukarov, *Russ. J. Electrochem.*, 2006, **42**, 689–698.
20 C. Alonso, M. J. Pascual and H. D. Abruna, *Electrochim. Acta*, 1997, **42**, 1739–1750.
21 B. Conway, H. Angerstein-Kozlowska, W. Sharp and E. Criddle, *Anal. Chem.*, 1973, **45**, 1331–1336.
22 W. Shao, G. Pattanaik and G. Zangari, *J. Electrochem. Soc.*, 2007, **154**, D201–D207.
23 L. Mascaro, S. S. Machado and L. Avaca, *J. Chem. Soc., Faraday Trans.*, 1997, **93**, 2577–2582.
24 C. Alonso, M. Pascual and H. Abruna, *Electrochim. Acta*, 1997, **42**, 1739–1750.
25 M. Palomar-Pardavé, E. Garfias-García, M. Romero-Romo, M. Ramírez-Silva and N. Batina, *Electrochim. Acta*, 2011, **56**, 10083–10092.
26 L. J. Buller, E. Herrero, R. Gómez, J. M. Feliu and H. D. Abruña, *J. Phys. Chem. B*, 2000, **104**, 5932–5939.
27 C. Cao and J. Zhang, *An introduction to electrochemical impedance spectroscopy*, Science Press, Beijing, 2002.
28 G. A. Ragoisha and A. S. Bondarenko, *Electrochim. Acta*, 2005, **50**, 1553–1563.
29 G. Ragoisha, *Electroanalysis*, 2015, **27**, 855–863.
30 M. Huang, J. B. Henry, P. Fortgang, J. Henig, N. Plumeré and A. S. Bandarenka, *RSC Adv.*, 2012, **2**, 10994–11006.
31 B. B. Berkes, A. Maljusch, W. Schuhmann and A. S. Bondarenko, *J. Phys. Chem. C*, 2011, **115**, 9122–9130.
32 B. Łosiewicz, R. Jurczakowski and A. Lasia, *Electrochim. Acta*, 2012, **80**, 292–301.
33 G. A. Ragoisha and A. S. Bondarenko, *Electrochem. Commun.*, 2003, **5**, 392–395.
34 G. Ragoisha, A. Bondarenko, N. Osipovich and E. Streltsov, *J. Electroanal. Chem.*, 2004, **565**, 227–234.
35 G. A. Ragoisha and A. S. Bondarenko, *Surf. Sci.*, 2004, **566**, 315–320.
36 X. Huang, Y. Chen, T. Fu, Z. Zhang and J. Zhang, *J. Electrochem. Soc.*, 2013, **160**, D530–D537.
37 L. Zhang, J. Fan, Z. Zhang, F. Cao, J. Zhang and C. Cao, *Electrochim. Acta*, 2007, **52**, 5325–5333.
38 L. Zhang, Doctoral Dissertation, Zhejiang University, 2008.
39 S. Machado, A. Tanaka and E. Gonzalez, *Electrochim. Acta*, 1991, **36**, 1325–1331.
40 A. J. Bard and L. R. Faulkner, *Electrochemical methods fundamentals and applications*, Y. H. Shao, G. Y. Zhu, X. D. Dong and B. L. Zhang, Chemical Industry Press, Beijing, 2nd edn, 2005.
41 A. Milchev and T. Zapryanova, *Electrochim. Acta*, 2006, **51**, 2926–2933.
42 A. Milchev and T. Zapryanova, *Electrochim. Acta*, 2006, **51**, 4916–4921.
43 M. Hölzle, U. Retter and D. Kolb, *J. Electroanal. Chem.*, 1994, **371**, 101–109.
44 M. Alanyalioglu, H. Çakal, E. Öztürk and Ü. Demir, *J. Phys. Chem. B*, 2001, **105**, 10588–10593.
45 M. Palomar-Pardave, I. González and N. Batina, *J. Phys. Chem. B*, 2000, **104**, 3545–3555.
46 A. Martínez-Ruíz, M. Palomar-Pardavé, J. Valenzuela-Benavides, M. H. Farías and N. Batina, *J. Phys. Chem. B*, 2003, **107**, 11660–11665.
47 L. H. Mendoza-Huizar, J. Robles and M. Palomar-Pardavé, *J. Electroanal. Chem.*, 2002, **521**, 95–106.
48 Y. Shingaya, H. Matsumoto, H. Ogasawara and M. Ito, *Surf. Sci.*, 1995, **335**, 23–31.
49 B. Y. Chang, E. Ahn and S. M. Park, *J. Phys. Chem. C*, 2008, **112**, 16902–16909.